Multi-Modal Medical Image Fusion using Multi-Resolution Discrete Sine Transform

VPS Naidu[1], M. Divya[2], P. Maha Lakshmi[3]

[1]Multi Sensor Data Fusion Lab, CSIR - National Aerospace Laboratories, Bangalore, India
[2] Dept. of ECE, JNTU College of Engineering, Ananthapuramu, India.
[3]Dept. of Instrumentation, VIT University, Vellore, India.
E-mail: vpsnaidu@gmail.com

Abstract: Quick advancement in high innovation and current medical instrumentations, medical imaging has turned into a fundamental part in many applications such as in diagnosis, research and treatment. Images from multimodal imaging devices usually provide complementary and sometime conflicting information. Information from one image may not be adequate to give exact clinical prerequisites to the specialist or doctor. Of-late, Multi-Model medical image fusion playing a challenging role in current research areas. There are many theories and techniques developed to fuse the multimodal images by researchers. In this paper, introducing a new algorithm called as Multi Resolution Discrete Sine Transform which is used for Multi-Model image fusion in medical applications. Performance and evaluation of this algorithm is presented. The main intention of this paper is to apply DST which is easy to understand and demonstrated method to process image fusion techniques. The proposed MDST based image fusion algorithm performance is compared with that of the well-known wavelet based image fusion algorithm. From the results it is observed that the performance of image fusion using MDST is almost similar to that of wavelet based image fusion algorithm. The proposed MDST based image fusion techniques are computationally very simple and it is suitable. The proposed MDST based image fusion algorithms are computationally, exceptionally basic and it is appropriate for real time medical diagnosis applications.

Keywords:-Multi resolution; DST; Image processing; Medical image fusion; Fusion quality evaluation metrics

1. Introduction

The objective of Computer Aided Diagnostic (CAD) system is to facilitate the early diagnosis, disease monitoring and better treatment [1]. Medical images provide essential information for CAD system. Image fusion could be a sub module in CAD system. Generally, image fusion can be classified into [2,3] I-Pixel level image fusion, inferring methods that go for the blend of the crude images from all the imaging sensors thought about 2). Highlight level image combination, inferring systems for extraction, mix of highlight vector from all considered imaging sensors and 3). Choice level image fusion, suggesting methods that go for the blend of the outputs of the groupings got on each imaging sensor. Of late, with rapid development of instrumentation technology, medical imaging has become an essential component in diagnosis, medical research and treatment. To get the accurate clinical information about the pathology "Multimodality medical images" are required. So that physicians can deal efficiently with diagnosis and evaluation. For the study of a given pathology Accumulation of numerous imaging data from imagery (MRI, SPECT, PET, X-ray, CT-scan) is required, the analysis of this data can be performed by clinician and provides appropriate medical decision or assist the physicians during a complicated surgical procedure based on his knowledge. Multimodality medical images generally provide complementary or conflicting information about the pathology. For instance, computed tomography scan (CT-Scan) report can provide bones and implants information with less distortion but it can't provide physical/biological changes, the magnetic resonance scan (MR-Scan) provide pathological soft tissue information but it can't provide bones and implants content. In this case physician can't get complete information about diseased parts only in one image; to avoid this multimodal medical image fusion is necessary. Hence, multimodal medical image fusion plays major role in challenging research areas [4, 5].

Multi Imaging sensor data fusion can be characterized as the way toward joining various images into a solitary image without loss of images information or

introduction of distortion [6].Fused image ought to contain all significant data than any individual source images. The combined image ought to be more appropriate for human visual and machine observation [7]. Some nonexclusive necessities forced on fusion scheme: 1) The fusion process ought to save all important data contained in the source images and 2) The fusion process not present any ancient rarities or irregularities which would interest the human onlooker or taking after handling stages and 3) superfluous components and noise ought to be stifled. The fusion of multimodal medical images frequently prompts extra clinical data not clear in individual source images. Another use of restorative image combination is that it can decrease the storage room by putting away the fused image as opposed to putting away different source images.

In this paper Pixel level image fusion is considering for intertwining the multimodal medical images, since the pixel level image fusion has the focal points that the images utilized contain the first measured amounts and the calculations utilized for combination are computationally straightforward and effective. The most straightforward image fusion is to take the normal of the grey level source images pixel by pixel. This method can create a few undesired impacts and reduced feature contrast. To overcome these type of problems, multi-scale changes can be done, for example, wavelets [8, 10-18], image pyramids [9, 19-22], spatial frequency [23], statistical signal processing [24,25] and fuzzy set theory [26] have been proposed. Real-world objects more often not contain structures at various scales or resolutions. Multi-determination or multi-scale methodologies can give a way to endeavour this reality and consequently multi-resolution image processing systems are widely utilized as a part of the advancement of image fusion strategies. Multi-resolution wavelet transform could give great restriction in both spatial and recurrence areas. Discrete wavelet transforms give directional data in disintegration levels and contain one of a kind data at various resolutions [5, 6]. In this paper, multi-resolution image analysis utilizing discrete sine transform (MDST) is introduced and assessed. MDST based multimodal restorative image combination calculation has been exhibited and contrasted its execution and surely understood wavelet based image combination method [16]. The thought is to apply basic and demonstrated procedure of DST for multi-resolution image fusion.

Image registration is one of the requirements to have the capacity to apply fusion techniques. The data in the images to be fused ought to be satisfactorily adjusted and enlisted prior to fusion. Here, it is expected that image registration is done for source images.

2. Discrete Sine Transform (DST)

Discrete Sine Transform is similar to Discrete Fourier Transform using real matrix. It is equivalent to imaginary parts of DFT of roughly twice the length. DST is operating on real data with odd symmetry, since the DFT of a real function is imaginary and odd function is odd. DST expresses of finitely discrete sequence in terms of sine functions oscillating at different frequencies. There are eight standard DST variants of which four are common and widely used for signal processing. Type-II DST is the most common variant of the discrete sine transform and it is simply called as DST. DST is a linear and invertible function.

The 1D (one dimensional) discrete sine transform $X(k)$ of signal $x(n)$ of length N is defined as [27-34].

2. 1 DST-I

$$X(k) = \sqrt{\frac{2}{N}} \sum_{n=0}^{N-1} x(n) \sin\left(\frac{\pi(n+1)(k+1)}{N+1}\right), \quad \begin{array}{l} 0 \le n \le N-1 \\ 0 \le k \le N-1 \end{array}$$

(1)

The DST-I is orthogonal and it is exactly equivalent to a DFT of real sequence that is odd around the 0th and middle points, scaled by 0.5. The DST-I is its own inverse.

2.2 DST-II

$$X(k) = \sqrt{\frac{2}{N}} \varepsilon_k \sum_{n=0}^{N-1} x(n) \sin\left(\frac{\pi(n+0.5)(k+1)}{N}\right)$$

(2)

$$\text{Where,} \quad \varepsilon_k = \begin{cases} \frac{1}{\sqrt{2}} & k = N-1 \\ 1 & \text{otherwise} \end{cases}$$

The inverse of DST-II is DST-III.

2.3 DST-III

$$X(k) = \sqrt{\frac{2}{N}} \varepsilon_n \sum_{n=0}^{N-1} x(n) \sin\left(\frac{\pi(n+1)(k+0.5)}{N}\right)$$

(3)

Where, $\varepsilon_n = \begin{cases} \dfrac{1}{\sqrt{2}} & n = N - 1 \\ 1 & \text{otherwise} \end{cases}$

The inverse of DST-III is DST-II.

2.4 DST-IV

$$X(k) = \sqrt{\frac{2}{N}} \sum_{n=0}^{N-1} x(n) \sin\left(\frac{\pi(n+0.5)(k+0.5)}{N} \right) \quad (4)$$

The DST-IV is its own inverse.

These DST types (DST-I to DST-IV) are related to real odd DFT's of even order. In fact, there are four additional DSTs (DST-V to DST-VIII) corresponding to real odd DFTs for odd order. However, these DSTs seem to be rarely used in signal analysis.

The 2D (two dimensional) discrete sine transform $X(k_1, k_2)$ of an image $x(n_1, n_2)$ of size $N_1 \times N_2$ is defined as [27-34]:

$$X(k_1, k_2) = \sqrt{\frac{2}{N_1}} \sqrt{\frac{2}{N_2}} \sum_{n_1=0}^{N_1-1} \sum_{n_2=0}^{N_2-1} x(n_1, n_2) \sin\left(\frac{\pi(n_1+1)(k_1+1)}{N_1} \right) \sin\left(\frac{\pi(n_2+1)(k_2+1)}{N_2} \right) \quad (5)$$

$$\text{where } 0 \le k_1, k_2 \le N_1 - 1, N_2 - 1$$

Similarly, the 2D inverse discrete sine trasnform is defined as:

$$x(n_1, n_2) = \sqrt{\frac{2}{N_1}} \sqrt{\frac{2}{N_2}} \sum_{k_1=0}^{N_1-1} \sum_{k_2=0}^{N_2-1} x(k_1, k_2) \sin\left(\frac{\pi(n_1-1)(k_1-1)}{N_1} \right) \sin\left(\frac{\pi(n_2-1)(k_2-1)}{N_2} \right) \quad (6)$$

$$\text{where } 0 \le n_1, n_2 \le N_1 - 1, N_2 - 1$$

One can see that there is no DC component in this transform unlike FFT and DCT. Both DST and IDST are separable transformations and the upside of this property is that 2D DST or 2D IDST can be obtained in two stages by progressive 1D DST or 1D IDST operations on columns followed by the resulting rows (or vice versa) of an image $x(n_1, n_2)$ as shown in eq.7 and this scheme is illustrated in Figure 1 [35-37].

$$X(k_1, k_2) = \sqrt{\frac{2}{N_2}} \sum_{n_2=0}^{N_2-1} \left[\sqrt{\frac{2}{N_1}} \sum_{n_1=0}^{N_1-1} x(n_1, n_2) \sin\left(\frac{\pi(n_1-1)(k_1-1)}{N_1} \right) \right] \sin\left(\frac{\pi(n_2-1)(k_2-1)}{N_2} \right) \quad (7)$$

3. Multi-Resolution Analysis

Multi-resolution image analysis utilizing discrete sine transform (MDST) is particularly like wavelet transform, where signal is filtered independently by low pass and high pass finite impulse response (FIR) channels and the output of each channel is decimated by a component of two to accomplish first level of disintegration. The decimated low pass filtered output is separated again independently by low pass and high pass FIR channels took after decimation by a factor of two provides second level of decomposition [36, 37]. The progressive levels of image disintegration can be accomplished by repeating the above said technique. FIR channels are supplanted with DST in the improvement of MDST.

3.1 Multi-resolution Image Decomposition:
The data stream chart of MDST (Single level deterioration) is appeared in Figure 2. The image which is to disintegrate is changed into frequency domain by applying DST in column wise. Low passed image 'L' can get by taking IDST on first 50% of focuses (1 to $0.5N$). So also, high passed image 'H' can get by taking IDST on second 50% of focuses ($0.5N$ to N) points. By applying the DST in row wise the low passed image 'L' is transformed into frequency domain. Take IDST on first 50% of focuses (in line shrewd) to get low passed image 'LL' and comparably take IDST on the remaining half to get the low-high passed image 'LH'. The high passed image 'H' is changed into frequency domain by applying DST row wise. Take IDST on initial half of focuses (in row wise) to get high-low passed image 'HL' and likewise take IDST on the staying half to get the high passed image 'HH'. The low passed image 'LL' contains the normal image data relating to low frequency band of multi scale decomposition. The low passed image 'LL' can be considered as smoothed and sub tested form of the source image. It represents the approximation of source image, 'LH', 'HL' and 'HH' and are definite sub images which

15

contain directional (horizontal, vertical and diagonal) data of the source image because of spatial introduction. Multi determination can be accomplished by recursively applying the above method to low pass coefficients (LL) from the past decay level. Image can be reproduced by turning around this strategy.

3.2 Performance Evaluation Metrics:

Since the reference (ground truth) image is available, the following reconstructed image quality evaluation metrics can be used to evaluate MDST performance.

3.2.1 Root Mean Square Error (RMSE)

This metric is computed as the root mean square error of the corresponding pixels in the reference image I_r and the reconstructed image I_c. This metric will be zero when the reference and reconstructed images are similar. This will increase when the dissimilarity increases.

$$RMSE = \sqrt{\frac{1}{MN}\sum_{y=1}^{M}\sum_{x=1}^{N}\left(I_r(x,y)-I_c(x,y)\right)^2} \quad (8)$$

Where, I_r is the reference image, I_c is the reconstructed image, (x,y) is a pixel index and M & N is the size of the image [38].

3.2.2 Percentage Fit Error (PFE)

PFE is computed as the norm of the difference between the corresponding pixels of reference and reconstructed/fusion image to the norm of the reference image. PFE will be zero when both reference and reconstructed images are exactly alike. PFE will increase when the reconstructed image is deviated from the reference image.

$$PFE = \frac{norm(I_r - I_c)}{norm(I_c)} * 100 \quad (9)$$

Where, $norm$ is the operator that is used to compute the largest singular value [38].

3.2.3 Mean Absolute Error (MAE)

$$MAE = \frac{1}{MN}\sum_{i=1}^{M}\sum_{j=1}^{N}\left|I_r(i,j)-I_c(i,j)\right| \quad (10)$$

Computed as the mean absolute error of the corresponding pixels in reference and reconstructed images [38].

3.2.4 Cross Correlation (CORR)

$$CORR = \frac{2C_{rc}}{C_r + C_c} \quad (11)$$

Where, $C_r = \sum_{i=1}^{M}\sum_{j=1}^{N}I_r(i,j)^2$ $C_f = \sum_{i=1}^{M}\sum_{j=1}^{N}I_c(i,j)^2$ and

$$C_{rc} = \sum_{i=1}^{M}\sum_{j=1}^{N}I_r(i,j)I_c(i,j)$$

CORR shows the correlation between the reference and reconstructed image. The ideal value of CORR is one when the reference and reconstructed are exactly alike and it will be less than one when the dissimilarity increases [38].

3.2.5 Signal noise Ratio (SNR)

$$SNR = 20\log_{10}\left(\frac{\sum_{i=1}^{M}\sum_{j=1}^{N}\left(I_r(i,j)\right)^2}{\sum_{i=1}^{M}\sum_{j=1}^{N}\left(I_r(i,j)-I_f(i,j)\right)^2}\right) \quad (12)$$

SNR will be high when the reference and reconstructed images are alike. Higher SNR value gives better results [39].

3.2.6 Peak signal to noise ratio (PSNR)

Its value will be high when the reconstructed and reference images are similar. Higher PSNR value implies better reconstruction. The peak signal to noise ratio is computed as:

$$PSNR = 10\log_{10}\left(\frac{L^2}{\frac{1}{MN}\sum_{y=1}^{M}\sum_{x=1}^{N}\left(I_r(x,y)-I_c(x,y)\right)^2}\right) \quad (13)$$

Where, L in the number of gray levels in the image [39].

Note: These evaluation metrics can be used for image fusion quality evaluation when reference image is available. Fused image will be used in place of reconstructed image.

3.3 MDST Results

The execution of MDST calculation is assessed and exhibited in this segment. Figure 3 demonstrates the ground truth image utilized as a part of multi-resolution analysis. In the first and second levels of disintegration of Figure 3 are appeared in Figure 4 utilizing DST-I. The recreated image from second level of deterioration utilizing DST-I is appeared in Figure 5a (left side) and the error image (distinction between the true image and the reconstructed image) is additionally appeared in Figure 5b (right side). One can assume that this reconstructed image is precisely coordinated with the ground truth image. It implies that there is no information loss for utilizing MDST for multi-resolution image analysis. Comparable

16

perception is produced using DST-II, DST-III and DST-IV comes about. The performance assessment measurements are appeared in Table1. It demonstrates that all DST calculations are performed practically comparable.

It is known that wavelet method trades spatial resolution at different scales. There is no trade-off, if DST is considered one can be obtained using the MDST at different scales of decomposition instead of applying DST on whole image.

4.Image Fusion

MDST based pixel level image fusion architecture is shown in Figure 6. One can observe that the modification of the present scheme is the use of MDST instead of wavelets or pyramids. The source images I_1 and I_2 which are to be fused are decomposed into D levels using MDST. The resultened decomposed images from I_1 and I_2 are

$$I_1 \rightarrow \left\{^1LL_D, \left\{^1LH_d, {}^1HH_d, {}^1HL_d\right\}_{d=1,2,...,D}\right\}$$
$$I_2 \rightarrow \left\{^2LL_D, \left\{^2LH_d, {}^2HH_d, {}^2HL_d\right\}_{d=1,2,...,D}\right\} \quad (14)$$

At every disintegration level d $(d=1,2,...,D)$, the combination manage will choose the bigger total estimation of the two detailed MDST coeficients, since the detailed coefficients compares more sharper brightness changes in the images, for example, edges and object boundaries and so on. These coefficients fluctuate around zero. At the coarsest level $(d=D)$, the combination govern take normal of the MDST estimate coefficients since the approximation coefficients at coarsest level are smoothed and sub-sampled version of the original image. The fused image I_f can be computed using equation (15):

$$I_f \leftarrow \left\{^fLL_D, \left\{^fLH_d, {}^fHH_d, {}^fHL_d\right\}_{d=1,2,...,D}\right\} (15)$$

4.1 Fusion Evaluation Metrics

In practice, both subjective and objective image fusion quality evaluation metrics can be used. In this paper, only objective evaluation metrics without reference image are used since reference image will not be available in real world applications. The following fusion quality metrics can be used to evaluate the performance of the fused algorithms when there are no reference images are available.

4.1.1   Standard Deviation (SD)

$$\sigma = \sqrt{\left(\frac{1}{MN}\sum_{y=1}^{M}\sum_{x=1}^{N}\left(I_f(x,y)-\mu\right)^2\right)} \quad (16)$$

Where, $I_f(x,y)$ is the pixel value of the fused image at the position (x,y) and μ is the mean value of the fused image.

SD is composed of the signal and noise parts of the image. SD is more efficient in the absence of noise in the image. SD measures the contrast in the fused image. An image with high contrast will have a high standard deviation [40].

4.1.2   Spatial Frequency (SF)
Spatial frequency criterion is: $SF = \sqrt{RF^2 + CF^2}$ (17)
Where, row frequency of the image:

$$RF = \sqrt{\frac{1}{MN}\sum_{x=1}^{M}\sum_{y=2}^{N}[I_f(x,y)-I_f(x,y-1)]^2}$$

Column frequency of the image:

$$CF = \sqrt{\frac{1}{MN}\sum_{y=1}^{N}\sum_{x=2}^{M}[I_f(x,y)-I_f(x-1,y)]^2}$$

SF indicates the overall activity level in the fused image. The fused image with high SF will be considered [38, 41, 42].

4.1.3   Information Entropy (He)
Entropy is used to measure the information content of an image. Using the entropy, the information content of a fused image is:

$$H = -\sum_{i=0}^{L}h_{I_f}(i)\log_2 h_{I_f}(i) \quad (18)$$

Where, $h_{I_f}(i)$ is the normalized histogram of the fused image $I_f(x,y)$ and L number of frequency bins in the histogram. Entropy is sensitive to noise and other unwanted rapid fluctuations. The information entropy measures the richness of information in an image. Hence, entropy is higher, performance is better [38].

4.1.4   Cross Entropy(Hc)
Cross-entropy is used to evaluate the similarities between input images and fused image. If there is a same content between fused image and reference image, then there will be low cross entropy. Hence, small cross entropy value corresponds to good fusion result. The overall cross entropy of the source images (I_1, I_2) and the fused image I_f is computed as:

$$CE(I_1,I_2;I_f) = \frac{CE(I_1;I_f)+CE(I_2;I_f)}{2} \quad (19)$$

17

Where, $CE(I_1; I_f)$ is the cross entropy of the image I_1 and the fused image I_f, and is computed as:

$$CE(I_1; I_f) = \sum_{i=0}^{L} h_{I_1}(i) \log\left(\frac{h_{I_1}(i)}{h_{I_f}(i)}\right)$$

Similarly $CE(I_1; I_f)$ is the cross entropy of the image I_2 and the fused image I_f and is computed as:

$$CE(I_2; I_f) = \sum_{i=0}^{L} h_{I_2}(i) \log\left(\frac{h_{I_2}(i)}{h_{I_f}(i)}\right)$$

Where, $h_{I_1}(i)$ is the normalized histogram of image I_1 and $h_{I_2}(i)$ is the normalized histogram of image I_2 [38].

4.1.5 Fusion quality index (FQI)
This metric would express the quality of the fused image given the source images as:

$$FQI = \sum_{w \in W} c(w)\left(\lambda(w)QI(I_1, I_f \mid w) + (1 - \lambda(w))QI(I_2, I_f \mid w)\right)$$

(20)

Where, $\lambda(w) = \dfrac{\sigma_{I_1}^2}{\sigma_{I_1}^2 + \sigma_{I_2}^2}$ computed over a window

$C(w) = \max\left(\sigma_{I_1}^2, \sigma_{I_2}^2\right)$ over a window

$c(w)$ is a normalized version of $C(w)$

$QI(I_1, I_f \mid w)$ is the quality index over a window for a given source image and fused image.
The range of this metric is 0 to 1. One indicates that the fused image contains all the information from the source images [38].

5. Results and Discussion

The objective of this paper is to fuse multimodal medical images using MDST. One can see that there is no ground truth (reference) image available. The multi-modal medical images used in this paper are taken from open literature [43-45].

5.1 Fusion of CT and MR images
Figure 7(i) and Figure 7(ii) demonstrate the CT and MR images separately. CT image gives clear bones data however it doesn't give delicate tissues data (see Figure 7(i)). The MR image gives delicate tissue data however it doesn't give bones data (see Figure 7(ii)).

It demonstrates that both CT and MR give reciprocal data. The combination of these two images, the resultant fused image now contains both the bones data and tissues data as appeared in Figure 8, which can't be found in the individual CT or MR image. Figure 8a demonstrates the fused images utilizing MDST-I with various levels of disintegrations. Figure 8b demonstrates the fused images with wavelets based image fusion technique. Fusion quality evaluation is appeared in Table 2. The qualities with intense shows better outcomes and the relating combination calculation is the best among other. From the figures and table, it is observed that the fused image contains all the important data. It is likewise watched that combination comes about by MDST are practically like that of wavelet based fusion results.

5.2 Fusion of T1-weighted MR and MRA Images
T1_weighted MR-image and MRA image with some illness are shown in Figure 9(i) and Figure 9(ii) respectively. In the Figure 9(i) it is clear that the soft tissue can recognize clearly and easily but the illness medical information has been lost from T1-weighted image. Whereas in MRA image the illness medical information (marked area) can recognize but the soft tissues are very difficult to discriminate because of its lower spatial resolution (see Figure 9(ii)). It shows the necessity of fusion of two images in order to provide complete medical information for the physician's analysis and diagnosis accurately. The fused image using DST-II and wavelets are shown in Figure 10a and Figure 10b respectively. The fusion quality evaluation metrics are shown in Table3.

5.3 Fusion of PET and CT images
The PET image and corresponding CT image are shown Figure 11(i) and (ii) respectively. PET can map biological function of an organ, detect subtle metabolic changes etc. CT provides the bone structure and soft tissues information. Fused image with MDST-I is shown in Figure 12a and with wavelet is shown in Figure 12b. Fusion quality evaluation metrics are shown in Table4. The fused image contained the information about biological function, metabolic changes, bone and soft tissue information.

5.4 Fusion of AF and IR images
In industrially developed countries, glaucoma is the most frequent cause of permanent blindness [45]. It is caused by an irreversible damage of the optical nerve and if it is not diagnosed in early stage, the damage to optical nerve may become permanent and

it may lead to blindness. Fusion of retinal auto fluorescence (AF) and infrared (IR) images may become promising loom for early diagnosis of the glaucoma. AF provides the information about hyper fluorescent zones (symptom of glaucoma in early stage and more visible periphery blood vessels. IR provides the information about the optical nerve head position, disc border, disc structure and blood vessels inside the optical disc [45]. Figure 13(i) shows the Auto fluorescence image and (ii) shows the IR image. The fusion of these two image using MDST-IV and wavelets are shown in Figure 14a &Figure 14b respectively. Without this fusion, the physician has to move his eye between AF and IR images to diagnose the glaucoma and it may be difficult to recognize the relationship among the patterns and objects. Fusion quality evaluation metrics are shown in Table5.

5.5 Fusion of MRI transverse and SPECT slices

The MRI transverse slice and corresponding SPECT image are shown in Figure 15(i) and (ii) respectively. SPECTS becomes an important clinical modality in oncology management. SPECT detects tumour with high sensitivity and high specificity but it does not offer anatomic details (see Figure 15(ii)). MRI is the most accurate imaging tool to evaluate the tumour size, location and shape. The fused images by MDST-II and wavelet are shown in Figure 16a &Figure 16b respectively. Fusion quality evaluation metrics are shown in Table 6. The fused images show the location of the tumour along with anatomical and biological information.

5.6 Fusion of CT Transverse and SPECT Slices

The CT transverse and SPECT slices are shown in Figure 17(i) and (ii) respectively. CT provides information regarding soft tissue and bony structure. Bone structure cannot be imaged by SPECT but is provides physiological or functional information. Combining these images can provide both bony structure and physiological or functional information in a single image instead of looking into two images as shown in Figure 18. The quality evaluation metrics are shown in Table7. It is observed that fusion algorithms with MDST (DST-I, DST-II, DST-III and DST-IV) and wavelet are performing almost similar.

Conclusion

An algorithm for multi-resolution image fusion using discrete Sine transform (MDST) has been presented and evaluated. The efficiency of MDST and IMDST for multi-resolution image processing has been tested. From the error image and the performance evaluation metrics, it is observed that there is no information loss by applying MDST on images. Different multimodal medical images from the literature have been used in this study. The performance of the proposed fusion algorithm has been compared with well-known wavelets based image fusion technique. Fusion algorithm with MDST is computationally very simple and it can be easily adoptable to medical image based diagnosis. It is observed that image fusion using MDST perform almost similar to that of wavelet based image fusion algorithm.

The MDST algorithm can be utilized to combine multi-aspects images too. Different orientation images ought to be registered before fusing them. In the event that the source images are in distinctive sizes, to fuse them the images should breakdown into various levels and wherever the sizes coordinate, then fusion process can perform. On the off chance that one of the source images is gray and other is colour image, then the coloured image must be converted into grey image and after that combination should be possible.

References:

1. Constantinos S. Pattichiset. Al., Medical Imaging Fusion Applications: An overview, IEEE, 2001.
2. J.A. Benediktsson, Introduction, Special issue on data fusion, IEEE Trans. Geo-science and Remote Sensing, Vol. 37, No.3, pp.1187, 1999.
3. S.T. Shivappa, B.D. Rao and M.M. Trivedi, An iterative decoding algorithm for fusion of multimodal information, EURASIP Journal of Advances in Signal Processing, Vol. 2008, Article ID 478396, 2008.
4. B. Barra, J.Y. Boire, A general framework for the fusion of anatomical and functional medical images, Neuro-Image, Vol. 13, No.3, pp.410-424, 2001.
5. Y.M. Zhu and S.M. Cochoff, An object-oriented framework for medical image registration, fusion and visualization, Computer Methods and Programmes in Biomedicine, Vol.82, No. 3, pp.258-267, 2006.
6. V.S. Petrovic and C.S. Xydeas, Gradient-based multi-resolution image fusion, IEEE Trans. On Image Proc., Vol. 13, No.2, pp.228-237, 2004.
7. Z. Zhang and R.S. Blum, A categorization of multi-scale-decomposition-based image fusion schemes with a performance study for a digital camera applications, Proceedings of the IEEE, vol. 87, No.8, pp.1315-1326, 1999.

8. Gonzalo Pajares and Jesus Manuel de la Cruz, A wavelet-based image fusion tutorial, Pattern Recognition, 37, 2007, pp.1855-1872.

9. P.J. Burt and R.J. Lolczynski, Enhanced image capture through fusion, In Proc. The 4th Int. Conf. on Computer Vision, pp. 173-182, Berlin, Germany, 1993.

10. S.G. Mallet, A theory for multi-resolution signal decomposition: The wavelet representation, IEEE Trans. Pattern Anal. Mach. Intel., Vol. 11(7), pp. 674-693, 1989.

11. H. Wang, J. Peng and W. Wu, Fusion algorithm for multi-sensor image based on discrete multi-wavelet transform, IEE Pro. Vis. Image Signal Process, Vol. 149 (5), 2002.

12. H. Li, B.S. Manjunath and S.K. Mitra, Multi-sensor image fusion using wavelet transform, Graph. Models Image Process, 57(3), pp.235-245, 1995.

13. T. Pu and G. Ni, Contrast-based image fusion using discrete wavelet transform, Opt. Eng., 39(8), pp.2075-2082, 2000.

14. D.A. Yocky, Image merging and data fusion by means of the discrete two-dimensional wavelet transform, J. Opt. Soc. Am. A, 12(9), pp.1834-1841, 1995.

15. J. Nunez, X. Otazu, O. Fors, A. Prades, V. Pala and R. Arbiol, Image fusion with additive multi-resolution wavelet decomposition: applications to spot1 landsat images, J. Opt. Soc. Am. A, 16, pp.467-474, 1999.

16. VPS Naidu and J.R. Raol, Pixel-Level Image Fusion using Wavelets and Principal Component Analysis – A Comparative Analysis, Defence Science Journal, Vol.58, No.3, pp.338-352, May 2008.

17. G.H. Qu, D.L.Zang and P.F. Yan, Medical image fusion by wavelet transform modulus maxima, J. of the Opt. Soc. Of America, vol.9, pp.184-190, 2001.

18. L.J. Chipman, T.M. Orr and L.N. graham, Wavelets and Image fusion, Proc. SPIE, vol2529, pp.208-219, 1995.

19. F. Jahard, D.A. Fish, A.A. Rio and C.P. Thompson, far/near infrared adapted pyramid-based fusion for automotive night vision, IEEE Proc. 6th Int. Conf. on Image Processing and its Applications (IPA97), pp.886-890, 1997.

20. B. Ajazzi, L. Alparone, S. Baronti and R. Carla, Assessment pyramid-based multi-sensor image data fusion, Proc. SPIE 3500, pp.237-248, 1998.

21. A. Akerman, Pyramid techniques for multisensory fusion, Proc. SPIE 2828, pp.124-131, 1992.

22. A. Toet, L.J. Van Ruyven and J.M. Valeton, Merging thermal and visual images by a contrast pyramid, Opt. Eng. 28(7), pp.789-792, 1989.

23. Shutao Li, James T. Kwok and Yaonan Wang, Combination of images with diverse focuses using the spatial frequency, Information fusion, 2(3), pp.167-176, 2001.

24. Rick S. Blum, Robust image fusion using a statistical signal processing approach, Information Fusion, 6, pp.119-128, 2005.

25. J. Yang and Rick S. Blum, A statistical signal processing approach to image fusion for concealed weapon detection, In IEEE Int. Conf. on Image Processing, Rochester, NY, pp.513-516, 2002.

26. AbdilhosseinNejatali and L.R. Ciric, Novel image fusion methodology using fuzzy set theory, Opt. Eng., 37(2), pp.485-491, 1998.

27. K. Rao and P. Yip, Discrete Cosine Transform, Algorithm, Advantages, applications, Academic Press, 1990.

28. M.V. Wicker hauser, Adaptive Wavelet Analysis from Theory to Software, Wellesley-Cambridge Press, Wellesley, MA, 1994.

29. S.A. Martucci, Symmetric Convolution and the Discrete Sine and Cosine transforms, IEEE Trans. Sig. Processing, SP-42, pp.1038-1051, 1994.

30. Vladimir Britanak, Patrick C. Yiop and K. R. Rao, Discrete cosine and Sine Transforms, Academic Press, 2007.

31. R.J. Clarke, Application of sine transform in image processing, Electronics Letters, Vol.19, No.13, pp.490-491, June 1983.

32. R.C. Gonzalez and P. Wintz, Digital Image Processing, MA: Addison-Wesley, 1987.

33. AK Jain, fast Karhunen-Loeve transform for a class of stocastic process, IEEE Trans on Comm, COM-24, pp.1023-29, 1976.

34. HB Kekra and JK Solanka, Compative performance of various trigonometric unitary transforms for transform image coding, International Journal of Electronics, Vol.44, pp.305-315, 1978.

35. Andew B. Watson and Allen Poirson, Separable two-dimensional discrete Hartly transform, J. opt. Soc. Am. A, Vol.3, No.12, pp.2001-04, Dec. 1986.

36. VPS Naidu, Discrete Cosine Transform-based Image Fusion, Special Issue on Mobile Intelligent Autonomous System, Defence Science Journal, Vol. 60, No.1, pp.48-54, Jan. 2010.

37. VPS Naidu, Multi-Resolution Image Fusion by FFT, ICIIP-2011, 3-5 Nov. 2011. (IEEE DoI: 10.1109/ICIIP.2011.6108862).

38. VPS Naidu, Girija G. and J.R. Raol, Evaluation of data association and fusion algorithms for tracking in the presence of measurement loss, AIAA Conference on Navigation, Guidance and Control, Austin, USA, 11-14, August 2003.

39. Gonzalo R. Arce, Nonlinear Signal Processing – A statistical approach, Wiley-Interscience Inc., Publication, USA, 2005.

40. Rick S. Blum and Zheng Liu, Multi-sensor image fusion and its applications, CRC Press, Taylor & Francis Group, NW, 2006.

41. A.M. Eskicioglu and P.S. Fisher, Image quality measures and their performance, IEEE Trans. Commu., 43(12), pp.2959-2965, 1995.

42. Shutao Li, James T. Kwok and Yaonan Wang, Combination of images with diverse focuses using the spatial frequency, Information Fusion, Vol. 2, pp. 169-176, 2001.

43. http://www.imagefusion.org accessed on 11th Nov. 2010

44. http://www.med.harvard.edu/AANLIB/home.html accessed on 11th Nov. 2010

45. RadimKolar, Libor Kubecka, and Jiri Jan, Registration and Fusion of the Auto-fluorescent and Infrared Retinal Images, International Journal of Biomedical Imaging, Volume 2008, Article ID 513478, pp.1-11, 2008

Table 1 Performance evaluation results

	RMSE	PFE	MAE	CORR	SNR	PSNR
DST-I	0	0	0	1	298.5752	176.0583
DST-II	0	0	0	1	296.5855	175.0635
DST-III	0	0	0	1	296.3264	174.9339
DST-IV	0	0	0	1	289.2224	171.3819

Table 2 Fusion quality evaluation metrics – fusion of CT and MR images

	Levels	H	SD	CE	SF	FQI
DST-I		2.0205	34.9334	1.4816	10.8784	0.6273
DST-II		2.0304	34.9177	1.4062	10.8800	0.6215
DST-III	L1	2.0217	34.9341	1.3607	10.8786	0.6273
DST-IV		2.0263	34.9278	1.3077	10.8767	0.6243
DTWT		2.0128	35.0047	1.4143	11.0919	0.6460
DST-I		2.0508	35.8253	0.8049	13.7920	0.5655
DST-II		2.0488	35.8011	0.8377	13.7801	0.5660
DST-III	L2	2.0498	35.8498	**0.7833**	13.8248	0.5671
DST-IV		**2.0527**	35.8363	0.7975	13.7961	0.5609
DTWT		2.0108	**36.0762**	1.0203	**13.9351**	**0.6724**

Table 3 Fusion quality evaluation metrics – Fusion of T1-weighted MR and MRA images

	levels	H	SD	CE	SF	FQI
DST-I		2.0668	0.1792	0.2449	0.0840	0.6003
DST-II		**2.1006**	0.1816	0.2636	0.0834	0.5968
DST-III	L1	2.0496	0.1794	0.2445	0.0839	0.6075
DST-IV		2.0139	0.1816	**0.2372**	0.0907	0.6324
DTWT		2.0053	0.1827	0.2419	0.0862	**0.6552**
DST-I		2.0973	0.1941	0.2576	0.1059	0.5887
DST-II		2.0944	**0.1988**	0.2574	**0.1116**	0.5872
DST-III	L2	2.0820	0.1875	0.2579	0.0992	0.5871
DST-IV		2.0861	0.1853	0.2552	0.1000	0.5846
DTWT		2.0213	0.1926	0.2396	0.1036	0.6475

Table 4 Fusion quality evaluation metrics – Fusion of PET and CT images

	levels	H	SD	CE	SF	FQI
DST-I		1.6198	0.1295	0.2724	0.0726	0.5962
DST-II		1.6375	0.1294	0.2505	0.0724	0.5948

		H	SD	CE	SF	FQI
DST-III	L1	1.6194	0.1294	0.2745	0.0725	0.5942
DST-IV		1.6380	0.1294	0.2525	0.0723	0.5942
DTWT		1.6675	0.1300	0.2388	0.0718	0.6314
DST-I		1.6472	0.1321	0.2528	0.0808	0.5995
DST-II		1.6677	0.1320	0.2352	0.0807	0.5992
DST-III	L2	1.6430	0.1321	0.2590	**0.0810**	0.5969
DST-IV		**1.6686**	0.1321	0.2377	0.0807	0.5972
DTWT		1.6635	**0.1331**	**0.2312**	0.0807	**0.6417**

Table 5 Fusion quality evaluation metrics – Fusion of AF and IR images

	Levels	H	SD	CE	SF	FQI
DST-I		7.1951	0.1746	2.0868	0.0839	0.6601
DST-II		7.2309	0.1746	1.9633	0.0840	0.6587
DST-III	L1	**7.2834**	0.1747	**1.8350**	0.0847	0.6609
DST-IV		7.2138	0.1747	2.1412	0.0851	0.6607
DTWT		7.2115	0.1752	2.1255	0.0833	0.6750
DST-I		7.2031	0.1789	1.9709	0.0968	0.6654
DST-II		7.2375	0.1785	1.8831	0.0956	0.6631
DST-III	L2	7.2743	0.1790	1.9290	0.0976	0.6682
DST-IV		7.2088	0.1788	2.0612	**0.0979**	0.6682
DTWT		7.2365	**0.1799**	2.0377	0.0964	**0.6867**

Table 6 Fusion quality evaluation metrics – Fusion of MRI transverse and SPECT slices

	levels	H	SD	CE	SF	FQI
DST-I		1.5684	0.1558	0.5987	0.0575	0.4687
DST-II		1.5808	0.1557	0.5720	0.0574	0.4639
DST-III	L1	1.5660	0.1558	0.5978	0.0575	0.4660
DST-IV		1.5759	0.1558	0.5985	0.0575	0.4655
DTWT		1.5165	0.1561	0.7082	0.0578	**0.5664**
DST-I		1.6130	0.1610	0.4490	**0.0732**	0.4475
DST-II		**1.6156**	0.1608	**0.4293**	0.0731	0.4478
DST-III	L2	1.6073	0.1609	0.4523	0.0731	0.4497
DST-IV		1.6111	0.1609	0.4454	0.0731	0.4501
DTWT		1.5257	**0.1615**	0.5899	0.0730	0.5656

Table 7 Fusion quality evaluation metrics – CT transverse and SPECT slices

	levels	H	SD	CE	SF	FQI
DST-I		1.5864	0.2553	0.5435	0.0598	0.4381
DST-II		1.5989	0.2552	0.5393	0.0599	0.4358
DST-III	L1	1.5844	0.2553	0.5497	0.0598	0.4377
DST-IV		1.5935	0.2552	0.5338	0.0598	0.4357
DTWT		1.5090	0.2556	0.5888	0.0612	**0.5825**
DST-I		1.6519	0.2578	0.4096	0.0774	0.4314
DST-II		**1.6561**	0.2578	0.4078	0.0774	0.4334
DST-III	L2	1.6529	0.2579	0.4077	0.0777	0.4314
DST-IV		1.6558	0.2579	**0.4075**	**0.0779**	0.4332
DTWT		1.5455	**0.2583**	0.5327	0.0774	0.4992
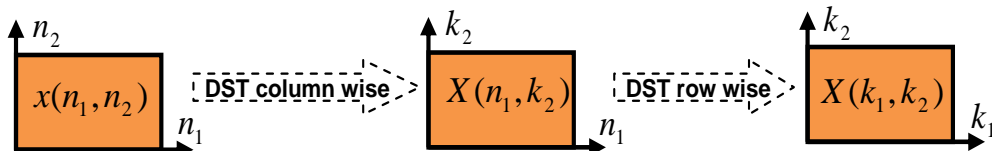
Figure 1: 2D DST implementation using separability property

a/r : along rows
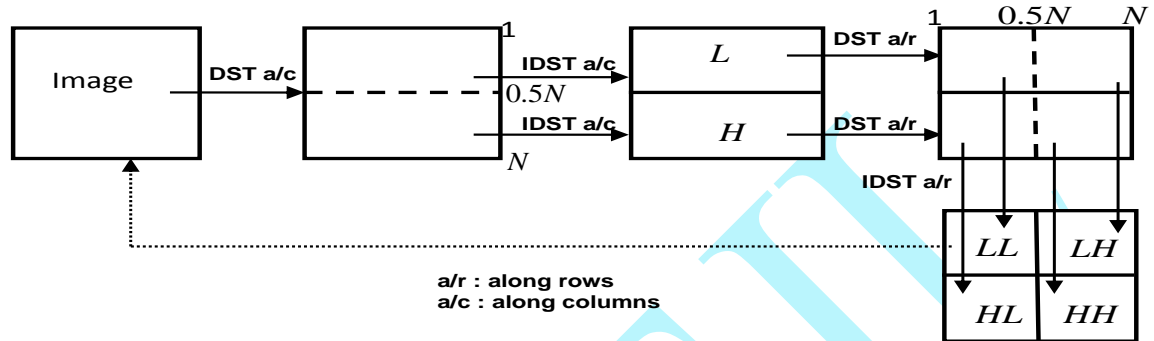a/c : along columns

Figure 2:Multi-resolution decomposition structures
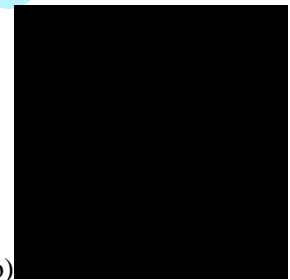

Figure 3: Ground truth image

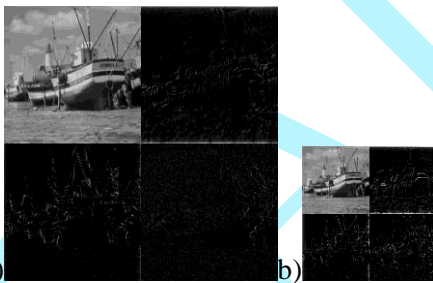Figure 5: a) Reconstructed image from 2nd level of decomposition and b) the error image DST-I

Figure 4a: First level of decomposition and b) Second
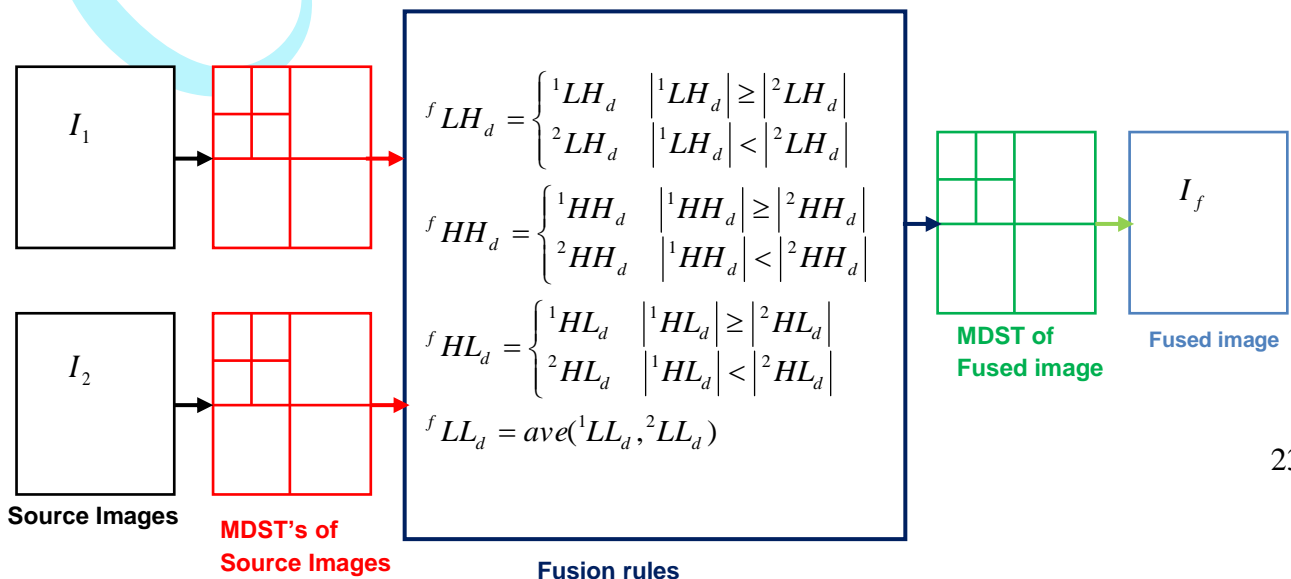level of decomposition using DST-I

$$^f LH_d = \begin{cases} ^1 LH_d & \left|^1 LH_d\right| \geq \left|^2 LH_d\right| \\ ^2 LH_d & \left|^1 LH_d\right| < \left|^2 LH_d\right| \end{cases}$$

$$^f HH_d = \begin{cases} ^1 HH_d & \left|^1 HH_d\right| \geq \left|^2 HH_d\right| \\ ^2 HH_d & \left|^1 HH_d\right| < \left|^2 HH_d\right| \end{cases}$$

$$^f HL_d = \begin{cases} ^1 HL_d & \left|^1 HL_d\right| \geq \left|^2 HL_d\right| \\ ^2 HL_d & \left|^1 HL_d\right| < \left|^2 HL_d\right| \end{cases}$$

$$^f LL_d = ave(^1 LL_d, ^2 LL_d)$$

I_1

I_2

Source Images

MDST's of
Source Images

Fusion rules

MDST of
Fused image

I_f

Fused image

23

Figure 6: Schematic diagram for MDST based pixel level image fusion scheme
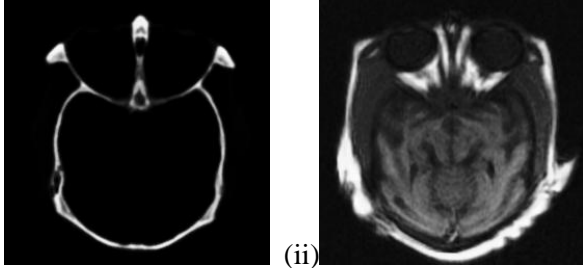
(ii)
Figure 7: (i) CT image and (ii) MR image

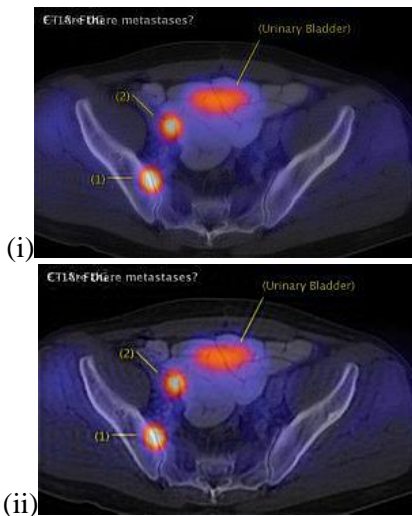(i)   (ii)
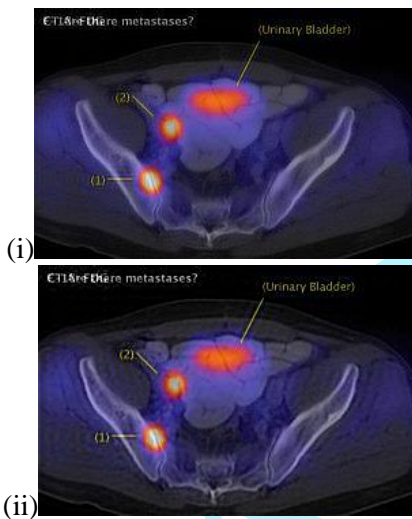Figure 10a: Fused image using DST-II with (i) one level and (ii) two levels of decompositions
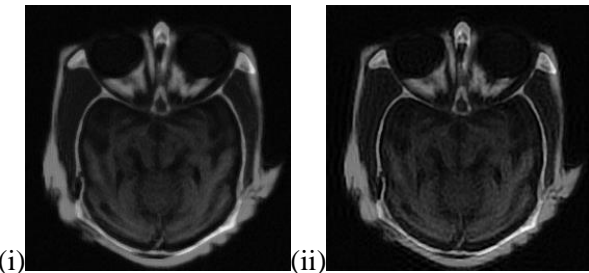
(i)   (ii)
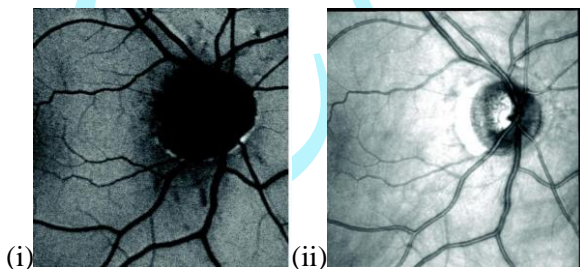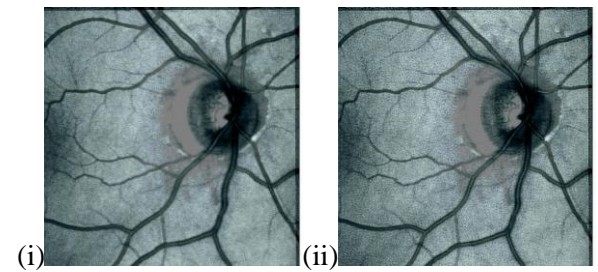Figure 8a: Fused image by DST-I with (i) one level and (ii) two levels of decompositions

(i)   (ii)
Figure 10b: Fused image using DTWT with (i) one level and (ii) two levels of decompositions
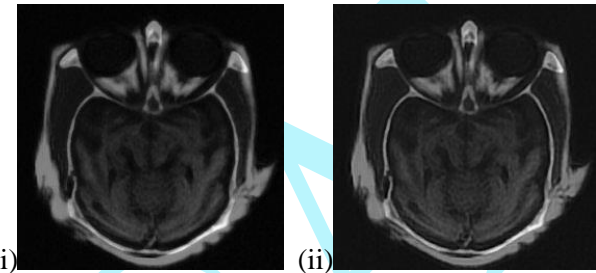
(i)   (ii)
Figure 8b: Fused image by DTWT with (i) one level and (ii) two levels of decompositions

(i)
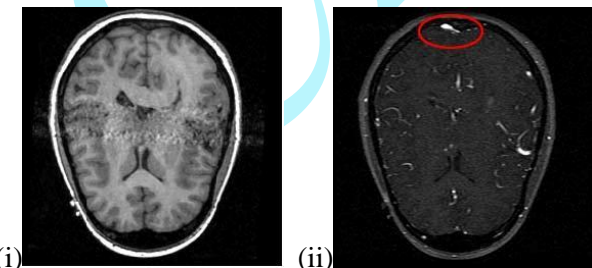
(i)   (ii)
Figure 9: (i) T1-weighted MR image and (ii) MRA image
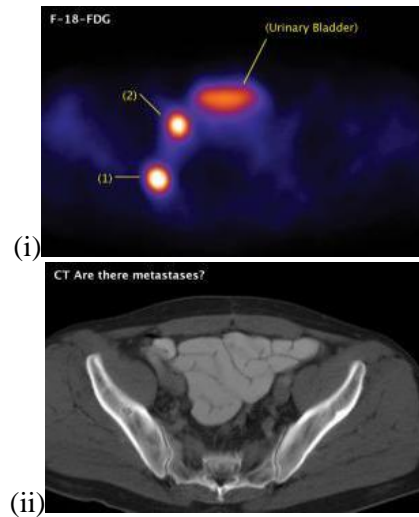
(ii)
Figure 11: (i) PET image and (ii) CT image

(i)

(ii)

Figure 12a: Fused image using DST-I with (i) one level and (ii) two levels of decompositions

(i)

(ii)

Figure 12b: Fused image using DST-III with (i) one level and (ii) two levels of decompositions

(i)

(ii)

Figure 13 (i) Auto fluorescence and (ii) IR images

(i)

(ii)

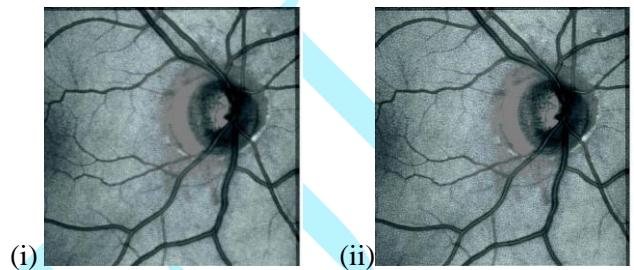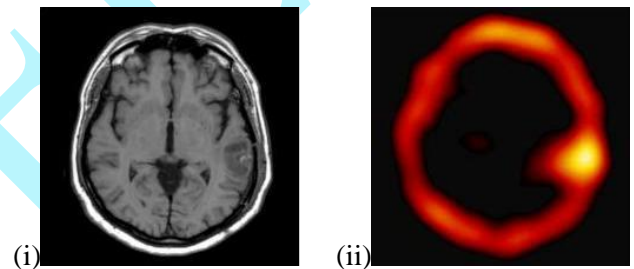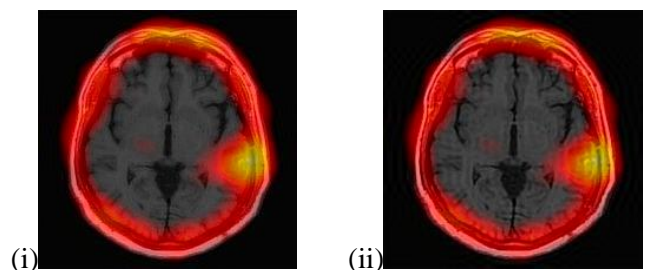Figure 14a: Fused image using DST-IV with (i) one level and (ii) two levels of decompositions

(i)

(ii)

Figure 14b: Fused image using DTWT with (i) one level and (ii) two levels of decompositions

(i)

(ii)

Figure 15 (i) MRI transverse and (ii) SPECT slices

(i)

(ii)

Figure 16a: Fused image using DST-II with (i) one level and (ii) two levels of decompositions
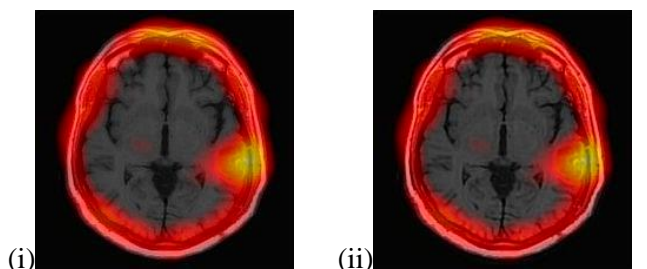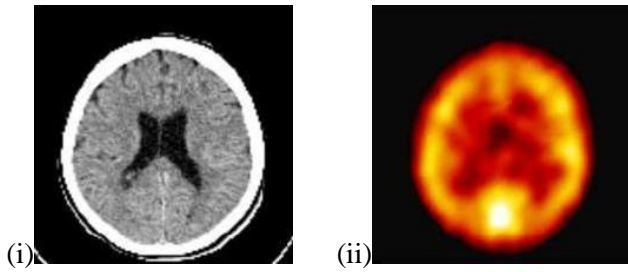

(i)

(ii)

Figure 16b: Fused image using DTWT with (i) one level and (ii) two levels of decompositions

(i)　　　　　　　　　(ii)

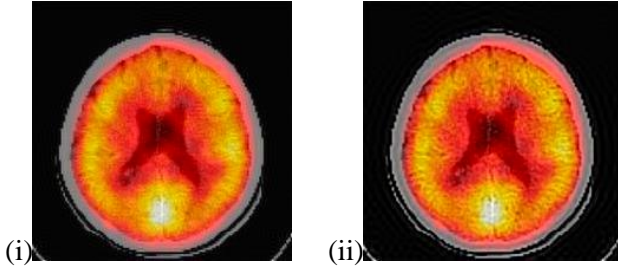Figure 17 (i) CT transverse and (ii) SPECT slices

(i)　　　　　　　　　(ii)

Figure 18a: Fused image using DST-II with (i) one
level and (ii) two levels of decompositions
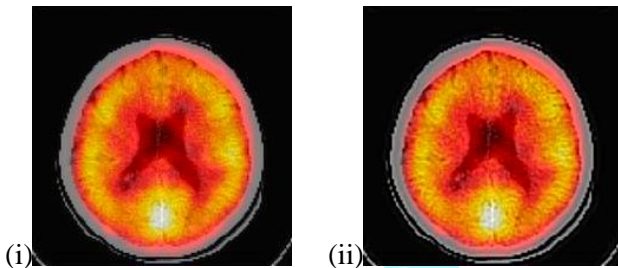

(i)　　　　　　　　　(ii)

Figure 18b: Fused image using DTWT with (i) one
level and (ii) two levels of decompositions